Tellus (1977), 29, 97–106

A note on some numerical experiments with model mountain barriers

By R. F. T. SMITH[1] and D. R. DAVIES, *Exeter University, North Park Road, Exeter, EX4 4QE, U.K.*

(Manuscript received November 10, 1975; in final form March 2, 1976)

ABSTRACT

A two-level, β-plane, quasi-geostrophic model in σ-coordinates has been used to study basic interactions between baroclinic instability waves and standing waves created by planetary scale topographic barriers. Numerical experiments over periods of 100 days were carried out, firstly with a flat topography and secondly with meridionally oriented mountain barriers of heights up to 2300 m. Two interesting results emerged: one was concerned with the computational aspect of modelling, the other with basic large scale dynamics.

The use of a centred differencing formulation of time dependent terms led to no computational difficulties in the case of flat topography, but with even a small barrier computational instability very quickly sets in. An Adams-Bashforth formulation entirely removes this instability.

The insertion of mountain barriers reproduced cyclogenesis in the lee of the barriers with similar primary dynamical characteristics to those found in complex model studies (e.g. Manabe & Terpstra, 1974).

1. Introduction

The importance is well known of the contribution of planetary scale mountain barriers to the main dynamical characteristics of the general circulation, to the preferred locations of cyclogenesis, and so to the fundamental mechanisms of climatic change. A review of the main theoretical studies in this field and a description of their important numerical experiments was given recently by Manabe & Terpstra (1974). They used a complex, nine-level general circulation model, developed at the Geophysical Fluid Dynamics Laboratory, with average January heating functions as a base. Comparison of results of numerical experiments with and without mountain barriers and the demonstration of a reduction in the transient component of global eddy kinetic energy function has thrown considerable light on planetary scale dynamics of the troposphere. The results of recent numerical studies by Egger (1974), using a β-plane, five-level, primitive equation, system, are also interesting. The integration domain was a channel, with cyclic boundary conditions on the eastern and western boundaries and a rigid wall at the northern and southern boundaries, with an orographic barrier placed in the channel.

A general dynamical problem in Meteorology on a given scale is to determine the primary factors on that scale and to formulate methods of parameterization of the contributions of smaller scale phenomena. In making a first approach to this aspect of the planetary scale mountain barrier problem by using a relatively simple model, we have modified a previous two-level model employed by Everson & Davies (1970) by expressing it in σ-coordinates and so conveniently reflecting the gross topographic barrier effects. The model was firstly integrated with no barriers and secondly with simulated, meridionally orientated, barriers, of heights up to 2300 m using two different separation distances of the barriers in the channel. A comparison of the calculated flow patterns and eddy kinetic energy functions for the different separations leads to interesting implications concerning the relationships between the different standing wave effects pro-

[1] Now with the British Aircraft Corporation, Stevenage, U.K.

duced and the baroclinic instability systems produced in the model integrations.

2. The model

The model used is basically a two-level, Phillips (1956) type system, but with pressure p replaced by $p/\pi = \sigma$, where π is the surface pressure. Surface boundary conditions can then be expressed conveniently on the actual ground surface. Following Phillips (1957) the velocity equations are then (using the standard modelling convention):

$$\frac{\partial u}{\partial t} + (\mathbf{V}\cdot\nabla)u - f_0 v = -\left(\frac{\partial \phi}{\partial x} + \frac{RT}{\pi}\frac{\partial \pi}{\partial x}\right) + A\nabla^2 u + \frac{g}{\pi}\frac{\partial \tau_x}{\partial \sigma} \tag{1}$$

$$\frac{\partial v}{\partial t} + (\mathbf{V}\cdot\nabla)v + f_0 u = -\left(\frac{\partial \phi}{\partial y} + \frac{RT}{\pi}\frac{\partial \pi}{\partial y}\right) + A\nabla^2 v + \frac{g}{\pi}\frac{\partial \tau_y}{\partial \sigma} \tag{2}$$

The continuity equation is

$$\frac{\partial}{\partial t} = -\nabla\cdot\left(\pi\int_0 \mathbf{V}\,d\sigma\right) \tag{3}$$

and the thermodynamic equation is

$$\left(\frac{\partial}{\partial t} + \mathbf{V}\cdot\nabla + \dot{\sigma}\frac{\partial}{\partial \sigma}\right)\log\theta = \frac{1}{C\,T}\frac{dQ}{dt} \tag{4}$$

where $\pi(x,y)$ is the presure on $\sigma = 1$, ϕ is the geopotential of a constant σ surface, and f_0 is taken to be a constant Coriolis parameter. The following assumptions are made:

(a) The terms $\dot{\sigma}(\partial u/\partial\sigma)$, $\dot{\sigma}(\partial v/\partial\sigma)$ are neglected in (1) and (2), even in the regions of mountain barriers. However, the computed vertical velocities are of similar magnitudes to those obtained in other systems.

(b) The factor RT/π is taken to be a constant; this is consistent with the geostrophic velocity assumption used,

$$\mathbf{v} = \left(\frac{1}{f_0}\right)\mathbf{k}\wedge\nabla(\phi + c\pi)$$

where $c = RT/\pi$, and ϕ is the geopotential of a σ surface. This leads to neglect of some terms in the vorticity equation, but some 40-day test integrations, with and without these terms, showed negligible differences.

(c) Static stability parameters, as expressed in Phillips type models, are assumed to be constant, although computer programmes could allow for spatial variations.

(d) In deriving a vorticity equation from (1) and (2), the term $\zeta(\nabla\cdot\mathbf{V})$ is neglected (the quasi-geostrophic assumption), but a $\dot{\sigma}$ field is generated at each time step through the thermodynamic equation.

(e) A difficulty in using σ-coordinate systems is that a momentum conserving scheme is not as easily ensured as in pressure coordinates. This can be overcome by using $\pi\mathbf{v} = \mathbf{V}$ as the dynamical variable in place of $\mathbf{v}$. However, the use of this variable in vorticity models leads to the introduction of several complicating terms through cross-differentiation. Due to limited computer facilities this has not been done in our system, but some numerical checks suggest the error is not serious, and, to ensure a simple model rather than ensure a mathematical exactness incompatible with other simplifying assumptions, the model is derived from the velocity eqs. (1) and (2).

Using similar substitutions to those employed in developing Phillips type models, the prediction equations at levels 1 and 3 ($\sigma = 0.25$ and $\sigma = 0.75$) are

$$\frac{\partial q_1}{\partial t} = -(\mathbf{V}_1\cdot\nabla)q_1 - \frac{R\lambda^2}{f_0 c_p}\dot{Q}_R - \beta v_1 + D_1 + F_1 \tag{5}$$

$$\frac{\partial q_3}{\partial t} = -(\mathbf{V}_3\cdot\nabla)q_3 + \frac{R\lambda^2}{f_0 c_p}\dot{Q}_R - \beta v_3 + D_3 + F_3 \tag{6}$$

where

$$q_1 = \zeta_1 - \lambda^2(\psi_1 - \psi_3) + \mu_1\pi,$$
$$\psi_1 = \phi_1/f_0, \quad \psi_3 = \phi_3/f_0 \tag{7}$$

$$q_3 = \zeta_3 + \lambda^2(\psi_1 - \psi_3) + \mu_3\pi \tag{8}$$

and $\dot{Q}_R$ is the radiative part of the heating function. The parameters

$$\mu_1 = -\frac{f_0}{\pi}\left\{1 - \frac{\kappa\theta_2}{(\theta_1-\theta_3)}\right\},$$

$$\mu_3 = -\frac{f_0}{\pi}\left\{1 + \frac{\kappa\theta_2}{(\theta_1-\theta_3)}\right\},$$

where $\kappa = R/C_p$, and

$$\lambda^2 = \frac{f_0\,\theta_2}{(\theta_1-\theta_3)(\phi_1-\phi_3)}$$

are constants. The diffusive and frictional terms are

$$D_1 = A\nabla^2\{\zeta_1 - \lambda^2(\Psi_1-\Psi_3)\},$$

$$D_3 = A\nabla^2\{\zeta_3 + \lambda^2(\Psi_1-\Psi_3)\},$$

$$F_1 = -k_2(\zeta_1-\zeta_3), \quad \text{and} \quad F_3 = -F_1 - k_3\zeta_4,$$

where A, k_2 and k_3 are appropriate constants.

The wind components calculated at the end of each time step, are given by

$$u_l = -\frac{\partial\psi_l}{\partial y} - c_l\frac{\partial\pi}{\partial y}$$

and

$$v_l = +\frac{\partial\psi_l}{\partial x} + c_l\frac{\partial\pi}{\partial x}, \quad \text{for } l = 1 \text{ and } 3.$$

The effect of variations of surface height is realized by assuming a linear profile of geopotential ψ with σ, and constraining ψ at $\sigma = 1$ to be the geopotential of the surface height; so that

$$\psi_1 = \tfrac{3}{2}\psi_D + \psi_4, \quad \text{and} \quad \psi_3 = \tfrac{1}{2}\psi_D + \psi_4$$

where ψ_4 is the "streamfunction" for the surface $(=\phi_4/f_0)$ and $\psi_D = \psi_1 - \psi_3$ is the streamfunction of the shear flow. The computing procedures used are then generally similar to those used by Everson & Davies (1970), apart from one important exception, discussed in section 3.

The integration domain used was effectively an infinitely long channel in the E–W direction, with cyclic boundary conditions on the E and W boundaries of the β-plane domains and rigid walls along the N and S boundaries. In the first series of experiments $n = 26$ grid points, spaced at 375 km intervals, were taken between the E and W "boundaries" of the basic β-plane region, with $m = 33$ grid points, spaced at 312.5 km, between the N and S boundaries. In a second series of experiments the E–W distance between the cyclic boundaries was doubled, the grid spacing remaining the same. The mountain barrier axis was taken to run in both sets of experiments N–S along the line of the $n = 7$ grid points, measuring from the W boundary and extending from $m = 8$ to $m = 26$ in the N–S direction, with width extending from $n = 4$ to $n = 10$. The contours of the barrier at 500 m, 1000 m, 1500 m, and 2000 m are shown in Fig. 4(a).

3. The computing scheme

The non-linear inertial terms in the velocity equations are expressed in an Arakawa (1966) finite difference system in order to suppress non-linear computational instability. The time differencing scheme was at first expressed in a centred form with implicit evaluation of the friction and diffusive terms. No computational instability problems were encountered with a flat lower boundary, but difficulties arose when surface height variations were included. Surface pressure and temperature contours showed small scale loops and kinks, and convergence of the iterative computer routines for surface pressure and streamfunction became excessively slow. No improvement was found when the maximum surface shape was smoothed and the problem still arose when topographic heights were reduced to one-tenth. Examination of the relative potential vorticities, surface pressure distribution, and streamfunction showed a "two-time step wave", which was amplifying (Fig. 1).

In order to consider the possibility that this computational instability might be initiated by a rapid adjustment of an initial zonal flow to a deflected flow around the barrier, the model was started from rest with the barrier already having been inserted. However, as the spurious computational wave still developed quickly, an alternative time differencing scheme was sought. The Adams-Bashforth method was eventually selected as it was easily programmed, reducing programme and storage requirements, and could be extended to give higher orders of accuracy. Expressing the basic

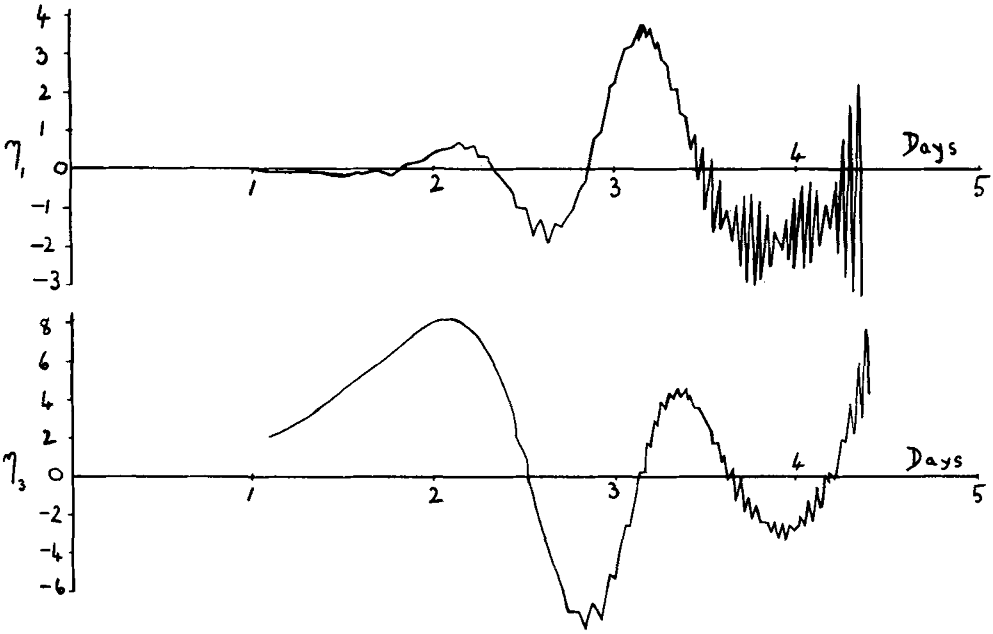

Fig. 1. Variations of the relative potential vorticities η_1 and η_3 at a point in the centre of the model domain (grid point $n = 13$, $m = 17$), when a centred time-differencing scheme is used. The initial flow was a uniform zonal current with a mid-latitude zonal velocity of 39 m/s at level 1 and 12.5 m/s at level 3. The lower boundary included a mountain barrier of maximum height of 2300 m, the peak being situated midway between equator and pole on the left-hand side of the domain and the barrier extending eighteen grid lengths in the north–south direction, six grid lengths in the east–west direction; the contours are shown in Fig. 4(a). η is in convenient arbitrary values.

differential equations to be solved in the form

$$\frac{dx}{dt} = f_i\,(x_1, x_2, \dots x_n, t)$$

where the x_i are the dependent variables of t, then if $x_i^{(n)}$, and $f_i^{(n)}$ denote the values of x_i and f_i at the time step n, an Adams-Bashforth method of integration is expressible as

$$x_i^{(n+1)} = x_i^{(n)} + (\tfrac{3}{2} f_i^{(n)} - \tfrac{1}{2} f_i^{(n-1)})\Delta t$$

A forward time step was also used every 10 days, in order to suppress the growth of further computational modes. The scheme proved satisfactory in suppressing computational instability, as seen in Fig. 2. We note that Edelmann (1972) has also discussed recently the problem of damping numerical instability caused by orography.

It was found to be computationally convenient in the model experiments to assume that the domain integral of relative potential vorticity, q (eqs. 7 and 8), should be conserved. This condition can be shown to depend on using cyclic E–W boundary conditions, the conventionally used boundary conditions at the N and S edges of the β-plane channel, conservation of total atmospheric mass, and the assumption that net heating of the atmosphere is zero. It is not of course automatically satisfied in the numerical model due to the accumulation of numerical errors. It is particularly important that this condition continues to apply, as it is assumed when finding the surface pressure and thermal streamfunction; without it the system of linear equations, which we attempted to solve numerically, are inconsistent. Since relaxation type methods are used, this is manifested by a gradual increase in the number of iterations required. It was found that the model could be amended to ensure this condition by continuously correcting the relative potential vorticity values by a small amount (about one part in 10^5 of a typical value); as a result, the number of iterations were reduced.

4. Discussion of results

The first numerical experiments, with integrations for 100 days, were performed with a model

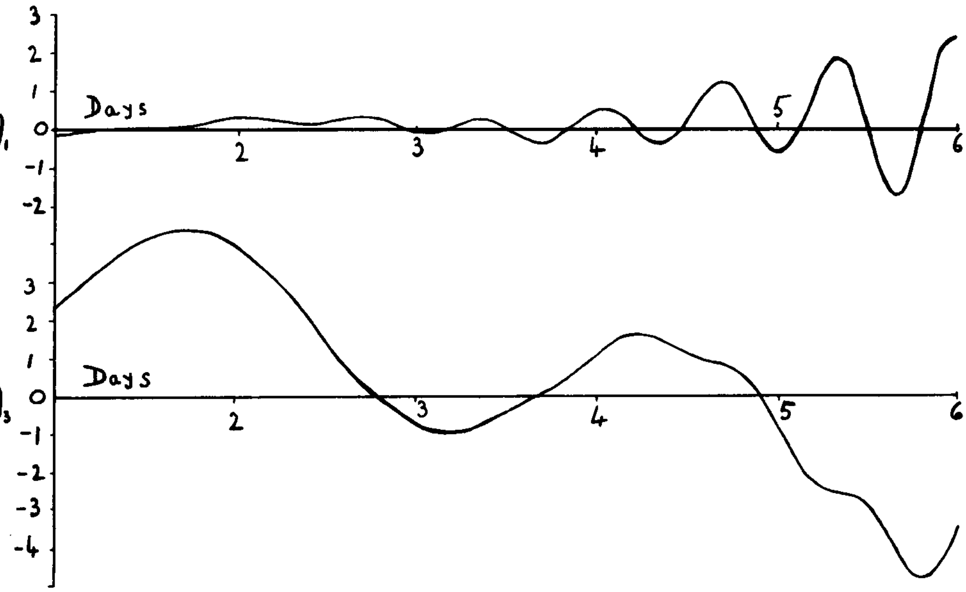

Fig. 2. Variations of the relative potential vorticities η_1 and η_3 as in Fig. 1 except that the Adams-Bashforth method has been used for the time differencing.

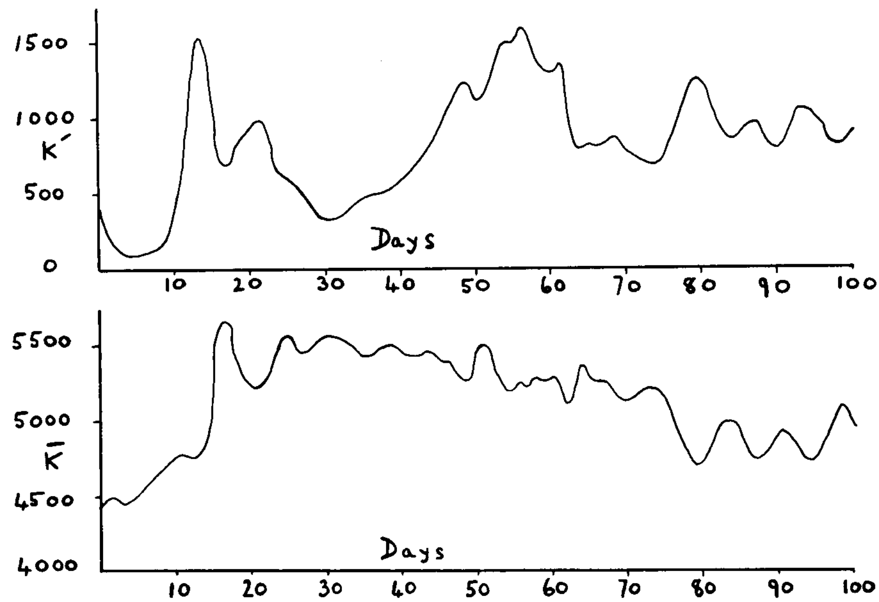

Fig. 3. Variations of domain eddy kinetic energy, K', and zonal kinetic energy, $\bar{K}$, using a flat lower boundary in the model. The units of K' and $\bar{K}$ are as defined by Phillips (1956), using convenient arbitrary values, independent of the number of grid points.

which had a flat lower boundary, and in which an initially zonal westerly flow with a vertical shear was disturbed by random perturbations of the surface pressure. The flow developed in a manner similar to that computed in an equivalent pressure coordinate model and the energy functions (eddy

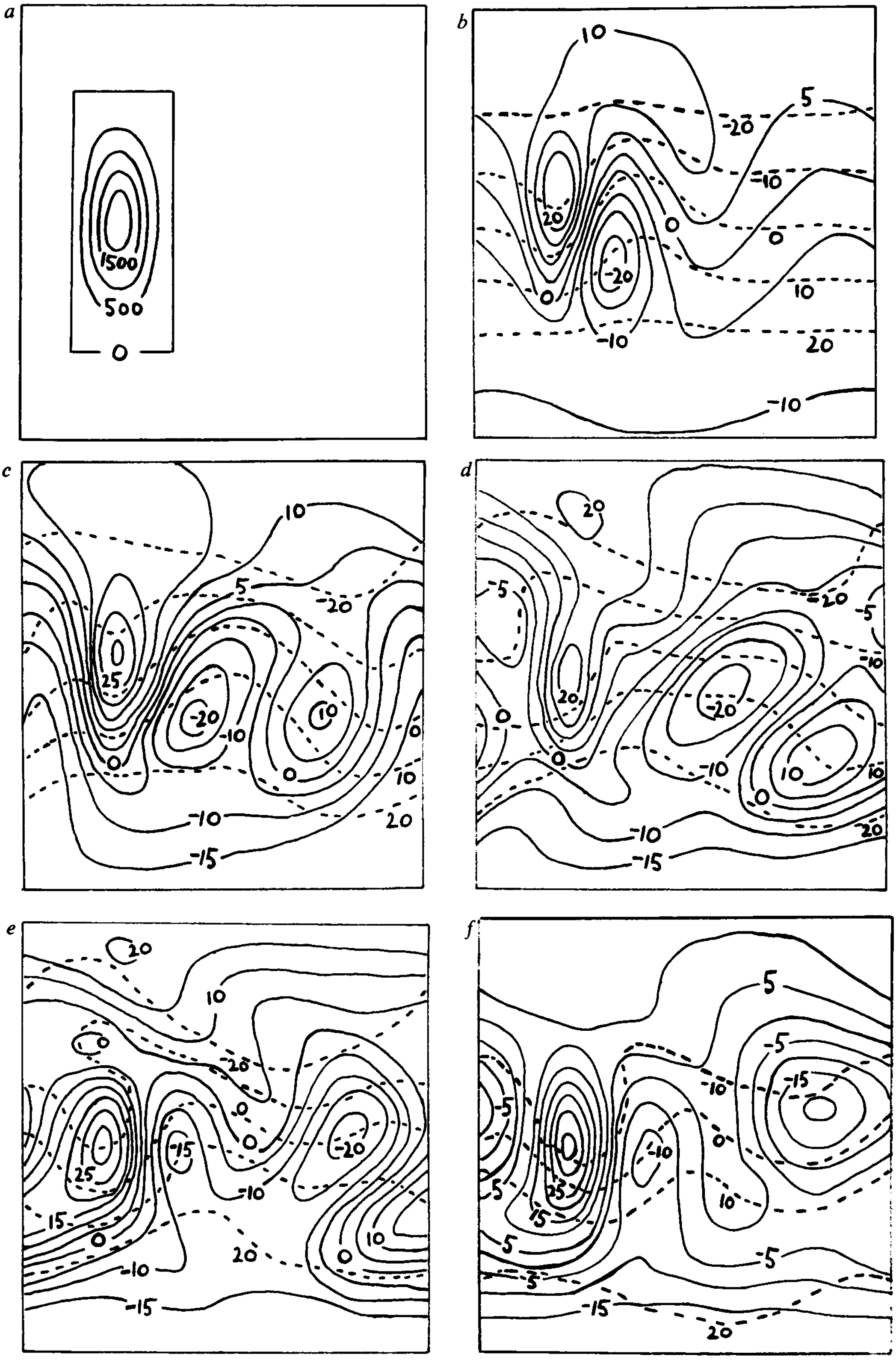
a
1500
500
0
b
10
5
-20
-10
20
0
-20
0
10
-10
20
-10
c
10
5
-20
0
25
-20
10
-10
0
0
0
10
20
-10
-15
d
20
-5
-20
-5
-10
20
0
-20
0
-10
10
10
0
-10
20
-15
e
20
10
0
-20
0
0
25
-15
-20
-10
15
0
10
20
0
-10
-15
f
5
-5
-10
-15
5
0
-10
0
5
25
10
15
5
-5
5
-15
20

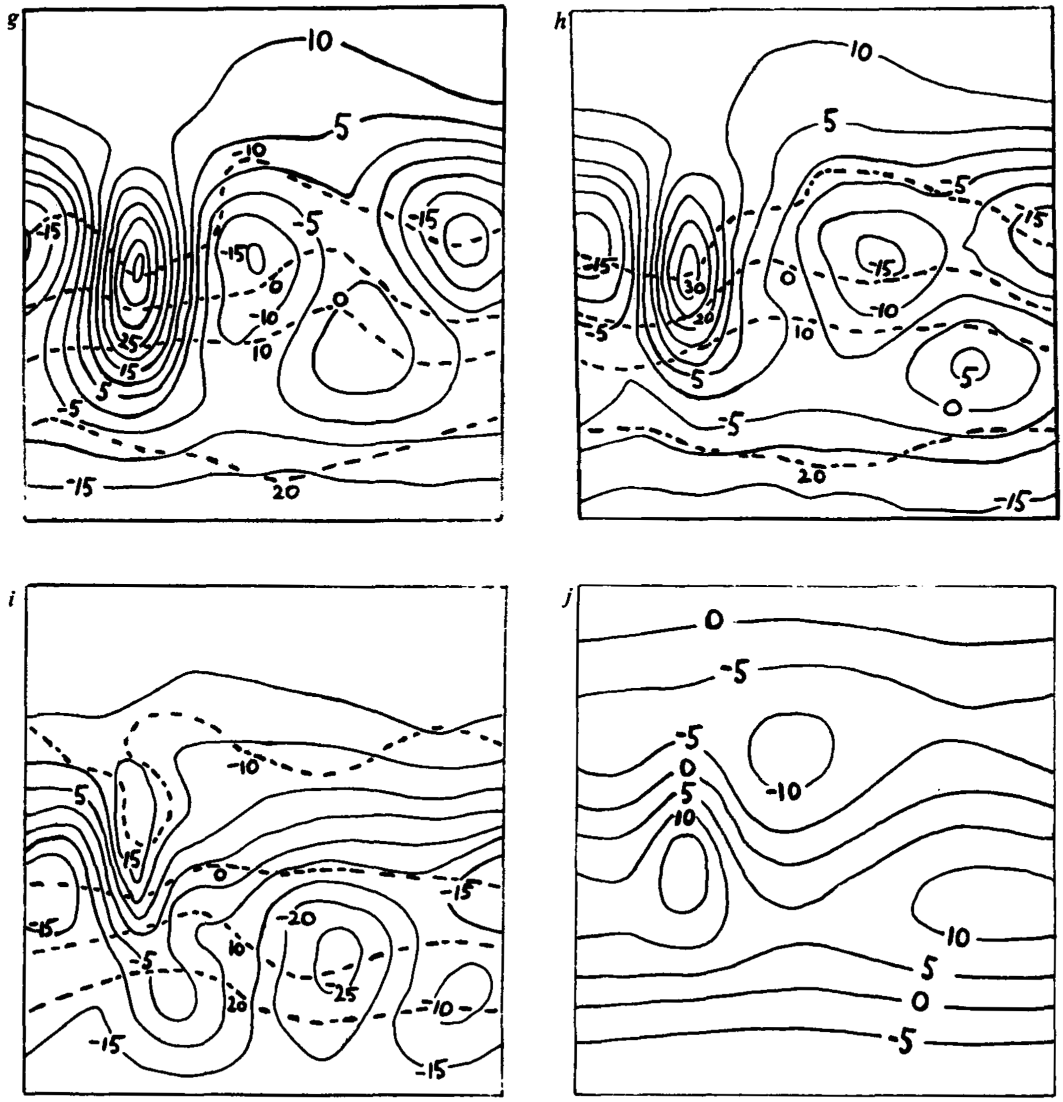

Fig. 4. Sample surface flow charts from a 100-day run in which a mountain of height 2300 m is included in the middle left-hand side of the domain, shown in Fig. 4(a). The charts show the flow *at the end* of the particular day indicated, the continuous lines representing surface pressure in mb (relative to 1000 mb). In addition, 500 mb temperature distributions in °C are shown dotted in Figs. (b), (c), (d), (e), (f), (g), (h), (i). (a) Contour heights of the mountain barrier at intervals of 500 m. (b) Day 0; Anticyclonic circulation is already apparent at the surface and in the lee of the mountain a cyclonic eddy system is formed. To the east of this, a ridge of high pressure is extending southwards. At Day 1 (not shown) this ridge extends further south whilst the "low" pressure system deepens. (c) By Day 2 the ridge has formed into a closed high pressure cell and these two systems begin to move eastwards appreciably. (d) By Day 3 the trough ahead of this high pressure system closes as it meets the fixed anticyclonic cell over the mountain. (e) At Day 4 a new "cyclonic" eddy system appears in the lee of the mountain and again high pressure extends south-eastwards ahead of it, whilst the "cyclonic" system, which had approached the mountain at Day 3, has been pushed to the north. The upper level flow has been split into two branches. At this stage, activity is fairly widely spread latitudinally over the domain. (f)–(h) At Days 38–40, flow near the pole is weaker and the "cyclonic" eddies no longer travel round the mountain. The low pressure system to the left of the chart remains on the westward side of the mountain as its centre moves further south. (i) At Day 97 "cyclonic" eddies continue to form in the lee of the mountain, but merge with the almost stationary trough when they have crossed the domain, and baroclinicity becomes restricted more and more to the south of the domain. (In the north a temperature wave visible at Day 97 was stationary since about Day 60.) (j) Time average distribution of surface pressure, averaged over Days 0 to 79.

kinetic energy K' and zonal kinetic energy, $\bar{K}$, defined as in Phillips, 1956) show a similar pattern of variations. After Day 70, the flow settles down to the characteristic index cycle, represented by oscillations in the eddy kinetic energy (as shown in Fig. 3). although the total kinetic energy is rather low and there is little activity in the northern region of the domain. This was felt to be due to the form chosen for the (500 mb) heating function (an adaptation of that used by Everson & Davies, 1970) which was improved in later experiments, producing higher values of the available potential energy in the model.

It was also noted that, in contrast to a case studied in which baroclinic activity was triggered off only by a land–sea heating differential (taking about 35 days of integration from an initial zonal state), the response of the system to the presence of a mountain barrier is rapid. For these experiments the model was initialized by adjusting the surface pressure, and streamfunction ψ_D, so that the flow was everywhere zonal (with the same characteristics as the flat surface runs). When a barrier with a peak of 2300 m was inserted with such a flow, baroclinic eddies were apparent within 2 days, and total eddy kinetic energy reaches a maximum after 10 days. As shown in Fig. 4, an anticyclonic flow system develops over the mountain and persists throughout the integration, its magnitude depending on the relative positions of the baroclinic systems and total eddy kinetic energy. An oscillation in the energy functions develops (shown in Fig. 5) with a period of about 5 days (the time taken for a "cyclone" to traverse the domain), caused by the interaction of the "baroclinic" waves with the standing waves formed by the presence of the mountain barrier. This formation of standing waves seems to have the interesting effect of inhibiting the growth of baroclinic instability waves by reducing the meridional temperature gradient which existed without the presence of the barrier: this suggests that the standing waves themselves transport heat to the polar region, thus reducing the requirement for meridional heat transport by baroclinic waves to achieve a climatological balance between tropical and polar model regions, although a diagnostic analysis of this effect has not yet been completed. The decrease in eddy kinetic energy towards the end of the 100-day integration is even more pronounced than in the flat case and eventually weak baroclinic activity is confined to the southern half of the domain. Further experiments,

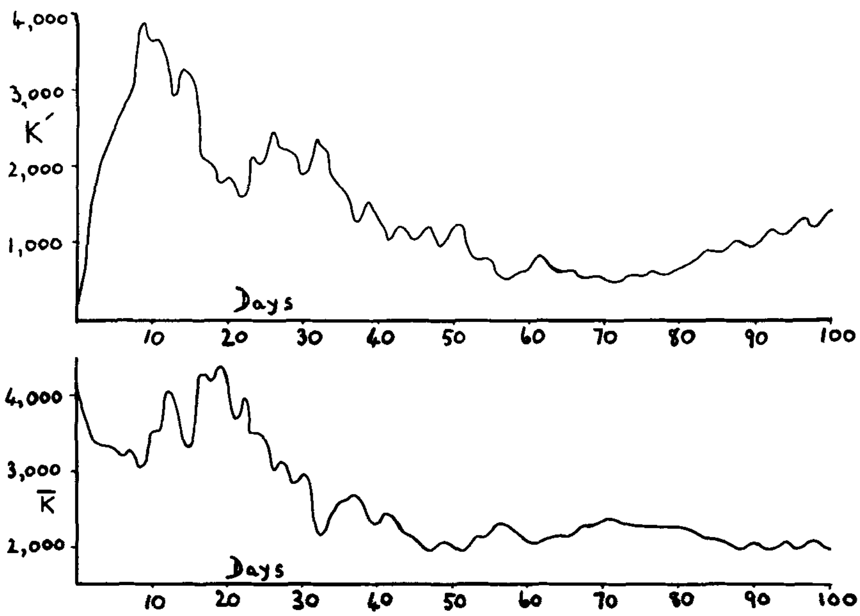

Fig. 5. Variation of eddy kinetic energy, K', and zonal kinetic energy, $\bar{K}$, (as defined by Phillips) using a mountain of height 2300 m situated midway between equator and pole, as shown in Fig. 4(a).

however, using a heating function with a 12% larger meridional gradient, led to higher values of eddy kinetic energy.

We noted also that, since a finite difference grid cannot adequately resolve a wave of less than four grid lengths, the mountain barrier effect necessarily occupies a large proportion of the domain of integration in the E–W direction. To provide a greater distance in which the baroclinicity may develop and to reduce the global effect of the mountain induced wave, experiments were carried out in which the E–W extent was doubled.

The dynamically interesting result of this doubling of the spacing between the barriers is that the magnitude of the global eddy kinetic energy function is almost restored to its initial value (see Fig. 6), suggesting that as the spacing of the barrier increases so the meridional transport effect of the standing waves decreases, and in order to achieve a climatological meridional heat balance the energy of the model cyclonic systems has to be increased. The nature of this dynamical problem is being further investigated by a further series of experiments using a variety of differently orientated barriers.

Finally, we note that the following main model characteristics obtained by Manabe & Terpstra using a complex nine level model are reproduced also by our very much simpler two-level, β-plane, channel flow model. Firstly, the surface flow charts (Fig. 4) show that a stationary trough is located in the lee of a planetary scale mountain range, oriented meridionally, with successive cyclonic eddies moving generally from SW to NE. Secondly, a major mountain range tends to increase the probability of cyclogenesis in the lee of these mountain ranges. This is illustrated by the 80-day, time averaged, surface pressure distribution shown in Fig. 4(j). Thirdly, the global eddy kinetic energy is seen to be reduced (Fig. 5) by the formation of standing waves created by planetary scale mountain barriers.

The model can be seen to have been developed now to a stage where dynamically interesting results are obtainable; the experiments can be extended by diagnostic analyses of model energy functions and heat transfer distributions to study the effect of geographic position, height, shape, and orientation of planetary scale barriers on interactions of the main model dynamical systems.

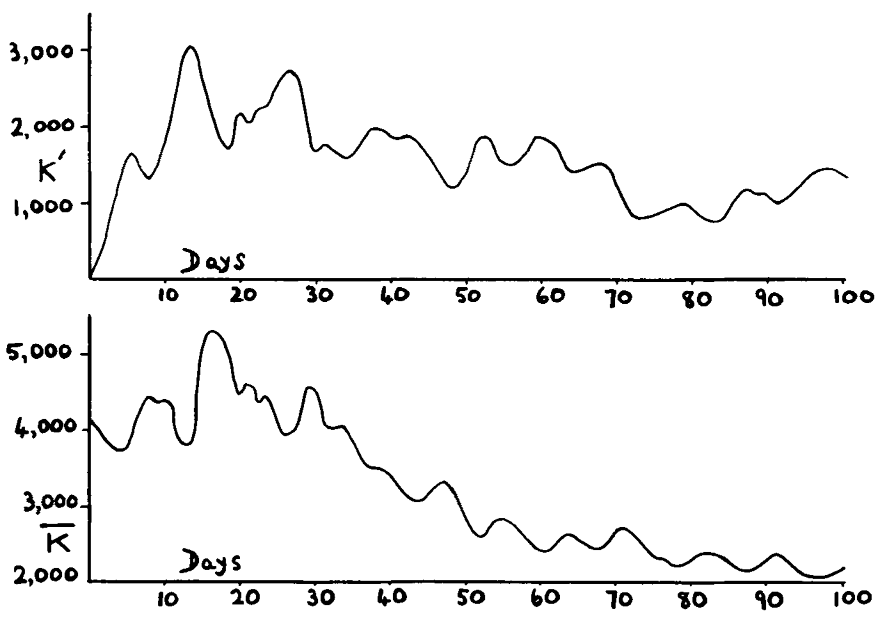

Fig. 6. K' and $\bar{K}$ variations with the mountain barrier positioned as in Fig. 5, but with the east–west extent of the domain doubled. The initial peak in K' is lower in this case as the wave caused by the mountain is reinforced less often. The energy function K' falls at a considerably slower rate than in Fig. 5.

5. Acknowledgements

We are grateful to the Natural Environmental Research council, U.K., for the award of a research grant which enabled Mr R. F. T. Smith to carry out the work. We are also grateful to Mr P. Langley, N.E.R.C. research student, for his assistance, particularly in the computational work leading to the preparation of some of the figures.

REFERENCES

Arakwa, A. 1966. Computational design for long-term numerical integration of the equations of fluid motion; two-dimensional incompressible flow. *J. Computational Phys. 1*, 119–143.

Edelmann, W. 1972. Initial balancing and damping of gravitational oscillations for forecast models including the orography. *Beitr. Phys. Atm. 45*, 94–120.

Egger, J. 1974. Numerical experiments on lee cyclogenesis. *Mon. Weather Rev. 102*, 847–860.

Everson, P. J. & Davies, D. R. 1970. On the use of a simple two-level model in general circulation studies. *Q.J.R. Meteorol. Soc. 96*, 404–412.

Manabe, S. & Terpstra, T. B. 1974. The effects of mountains on the general circulation of the atmosphere as identified by numerical experiments. *J. Atmos. Sci. 31*, 3–42.

Phillips, N. A. 1956. The general circulation of the atmosphere; a numerical experiment. *Q.J.R. Meteorol. Soc. 82*, 123–164.

Phillips, N. A. 1957. A coordinate system having some special advantages for numerical forecasting. *J. Meteorol. 14*, 184–185.

ЗАМЕЧАНИЕ О ЧИСЛЕННЫХ ЭКСПЕРИМЕНТАХ С МОДЕЛЬНЫМИ ГОРНЫМИ ПРЕПЯТСТВИЯМИ.

Двухуровенная, квазигеострофическая модель на β-плоскости в σ-координатах используется для изучения взаимодействия между волнами, возникающими за счет бароклинной неустойчивости, и неподвижными волнами, создаваемыми топографическими препятствиями планетарного масштаба. Были проделаны численные эксперименты с интегрированием на 100 дней, сначала с плоской топографией, а затем с мерндионально ориентированными горными препятствиями высотой до 2300 м. Получены два интересных результата: один касается вычислительных аспектов моделирования, другой-крупномасштабной динамики.

Использование схемы центральных разностей по времени не приводит к вычислительным трудностям в случае плоской тоиографии, в то же время даже малое препятствие приводит к быстрому возбуждению неустойчивости. Схема Адамса —Башфорта целиком подавляет эту неустойчивость. Введение горных препятствий приводит к циклогенезу за препятствием с главными динамическими характеристиками, похожими на результаты более сложных моделей (например, Манабе и Терпстра, 1974).